Robust Eulerian-on-Lagrangian Rods

ROSA M. SÁNCHEZ-BANDERAS, Universidad Rey Juan Carlos
ALEJANDRO RODRÍGUEZ, SEDDI Labs
HÉCTOR BARREIRO, Universidad Rey Juan Carlos
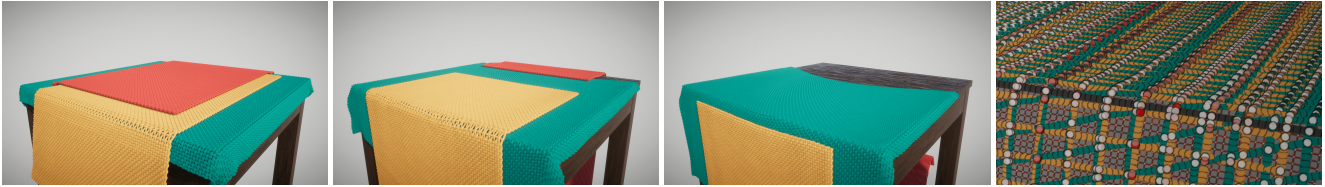MIGUEL A. OTADUY, Universidad Rey Juan Carlos

Fig. 1. Simulation of three yarn-level tablecloths stacked on top of each other. We handle both intra-fabric and inter-fabric contacts implicitly with our novel Eulerian-on-Lagrangian (EoL) simulation. Frictional contact is correctly handled, even under extreme sliding and crossing of yarns. We introduce novel EIL nodes to handle robustly pervasive degeneracies in the discretization. The rightmost image shows the soup of nodes around the edge of the table. White dots represent contacts between standard EoL nodes, red dots contacts between our novel EIL nodes, and pink dots contacts between EoL and EIL nodes.

This paper introduces a method to simulate complex rod assemblies and stacked layers with implicit contact handling, through Eulerian-on-Lagrangian (EoL) discretizations. Previous EoL methods fail to handle such complex situations, due to ubiquitous and intrinsic degeneracies in the contact geometry, which prevent the use of remeshing and make simulations unstable. We propose a novel mixed Eulerian-Lagrangian discretization that supports accurate and efficient contact as in EoL methods, but is transparent to internal rod forces, and hence insensitive to degeneracies. By combining the standard and novel EoL discretizations as appropriate, we derive mixed statics-dynamics equations of motion that can be solved in a unified manner with standard solvers. Our solution is simple and elegant in practice, and produces robust simulations on large-scale scenarios with complex rod arrangements and pervasive degeneracies. We demonstrate our method on multi-layer yarn-level cloth simulations, with implicit handling of both intra- and inter-layer contacts.

1 INTRODUCTION

The simulation of rods has been extensively studied in computer graphics. This is not surprising, as many daily-life objects are composed of rod-like structures, such as ropes [Bergou et al. 2008; Pai 2002], chains, belts, cloth [Kaldor et al. 2008], cables [Servin

Authors' addresses: Rosa M. Sánchez-Banderas, Universidad Rey Juan Carlos, rosanban@gmail.com; Alejandro Rodríguez, SEDDI Labs, alejandro.rodriguez@seddi.com; Héctor Barreiro, Universidad Rey Juan Carlos, hecbarcab@gmail.com; Miguel A. Otaduy, Universidad Rey Juan Carlos, miguel.otaduy@urjc.es.

et al. 2010], hair [Selle et al. 2008], tendons [Sachdeva et al. 2015], spaghetti, or even fluid filaments [Bergou et al. 2010].

Rod simulations become particularly challenging under complex contact arrangements, as their small cross-section makes them vulnerable to collision handling errors. But when contacts persist over time, with rods sliding with respect to each other, Eulerian-on-Lagrangian (EoL) discretizations [Sueda et al. 2011] offer an attractive approach to gain robustness in contact handling, at the expense of a slightly more complex derivation of the equations of motion. EoL methods augment the classic Lagrangian discretization of deformable solids with Eulerian coordinates that allow nodes to move in the material domain. The power of EoL methods is the ability to track explicitly contact points both in the spatial and material domains, simply by placing nodes at contact locations, and thus reduce the complexity and increase the accuracy of contact handling.

However, we have observed that existing EoL works exploit only moderately this power. To the best of our knowledge, none of them shows multiple stacked layers of rods or shells sliding with respect to each other. As we discuss in detail later in Section 3, there is a fundamental reason for this. With sliding contacts, EoL discretizations easily become degenerate. To avoid simulation instabilities, previous EoL works use remeshing, but this strategy cannot be used under multiple stacked layers, when the geometry of the contact configuration is intrinsically degenerate, with contacts crossing each other.

We present a simulation method that handles robustly degenerate discretizations in EoL rods. Our method does not use remeshing; it relies instead on a formulation of equations of motion that is insensitive to degenerate elements. As a result, we can simulate stacks of rods sandwiched between sliding contacts, with nodes constantly crossing each other in the material domain, all with implicit contact handling enabled by the EoL approach.

The key to our solution is a type of mixed Eulerian-Lagrangian discretization node, carefully designed to support accurate and efficient modeling of contact interactions as in EoL methods, but transparent

to the modeling of internal rod forces, and hence insensitive to degeneracies in the discretization. In Section 3 we describe this type of node, which we call *Eulerian with Interpolated Lagrangian* (EIL in short), and we discuss its beneficial properties.

Based on a combination of the new EIL and regular EoL discretizations, we have designed a simple and elegant algorithm to derive robust equations of motion at runtime. The strategy is to replace offending EoL nodes with EIL nodes, and skip EIL nodes in the definition of internal forces. Our algorithm, described in Section 4, yields a combination of dynamics and statics equations, which can be solved in a unified manner with standard solvers.

In our results, we show the application of our solution to challenging simulations of yarn-level cloth. Beyond single woven or knit fabrics [Cirio et al. 2014, 2017], we extend the power of EoL methods to stacked layers of fabrics, by handling implicitly both intra-fabric as well as inter-fabric contacts. We demonstrate results on several familiar settings: tablecloth layers, pant pockets, and shirt tags. We also show that our method enables scalable EoL-based simulation of complex knit fabrics where multiple yarns slide and cross each other. To date, these fabrics could be handled only through traditional Lagrangian methods with explicit contact handling [Kaldor et al. 2008], assuming periodicity to predict the relaxed pattern shapes [Leaf et al. 2018]. The combined simplicity and effectiveness of our solution leads to an elegant implementation and robust results, despite ubiquitous discretization degeneracies as shown in Fig. 1. While we only demonstrate our ideas on rods, we believe that the core concepts can also be extended to other EoL domains such as thin shells [Weidner et al. 2018].

2 RELATED WORK

Before describing our method in depth, we briefly overview related work on rod models, yarn-level cloth simulation, other EoL methods, and contact handling of cloth and hair stacks.

Eulerian-on-Lagrangian Methods. Fan et al. [2013] coined the term "Eulerian-on-Lagrangian" to denote simulations that use both Eulerian and Lagrangian coordinates to define aggregate kinematics. They used their method to combine large rigid or modal motion with robust deformation on Eulerian grids. In their setting, the combined Eulerian and Lagrangian kinematics yield an ambiguous representation, which is resolved by minimizing the Eulerian contribution.

Earlier, however, Sueda et al. [2011] had introduced an EoL method for the simulation of rods in contact with other objects. Their method places nodes with both Eulerian and Lagrangian coordinates at contact locations, and ensures that rod bending is accurately and efficiently resolved even when contacts slide. The method of Sueda et al. forms the basis for our work, and we provide a more extensive discussion of its benefits and limitations in Section 3.

Similar EoL methods have been designed for the simulation of skin sliding on top of the body [Li et al. 2013], or the interaction of tendons with phalanges in hand biomechanics [Sachdeva et al. 2015]. EoL cloth [Weidner et al. 2018] extends Sueda's rod discretization to cloth modeled as a thin shell. By setting discretization nodes at sharp contacts, simulations avoid locking and spurious energy artifacts. EoL cloth uses conformal remeshing to maintain good mesh quality while contact nodes slide in the material domain. However, in the

examples shown by the authors, contact nodes are sparse, and there are no sandwiched contacts or multiple stacked cloth layers, hence contact nodes never approach and cross each other. Contrary to their examples, remeshing is not an option in cases where degeneracies are intrinsic to the contact geometry, such as the ones we handle in our work.

Deformable Rods. Rods, strands, or deformable curves in general have been simulated using diverse methods. Earlier approaches relied on mass-spring systems due to their simplicity [Rosenblum et al. 1991], but these methods have been adapted to fit the needs of production animations not long ago [Iben et al. 2013; Selle et al. 2008]. Other methods represent rods as curves with adapted frames. A popular approach is to use an explicit representation of the center line, by discretizing the Cosserat geometry model [Pai 2002; Spillmann and Teschner 2007]. Then, additional constraints must be introduced to enforce inextensiblity. Bergou et al. [2008] introduced the discrete elastic rod model, where an oriented frame remains always naturally adapted to the center line thanks to a curve-angle parameterization. In our examples, we use a twist-free elastic rod model, but any of the methods above could be integrated to model twist, as they all discretize the center line explicitly. An alternative is to represent the center line implicitly using a reduced-coordinate formulation based on curvatures and twist [Bertails et al. 2006].

Some methods consider adaptive discretizations of rods to accurately resolve contacts. One possibility is to resample rods while minimizing the energy difference [Spillmann and Teschner 2008], and another possibility is to introduce nodes based on the tension of the rod [Servin et al. 2010]. EoL methods [Sueda et al. 2011] can also be regarded as adaptive discretizations, where contact-based adaptivity is achieved by sliding nodes in the material domain.

Yarn-Level Cloth. Rod models are also used in computer graphics for the simulation of cloth at the yarn level. While costly, due to the massive number of yarns in real garments, yarn-level models offer the ability to reproduce, by construction, the structural nonlinearity and anisotropy of fabrics. Kaldor et al. [2008] introduced the first method to simulate complete pieces of cloth at the scale of yarns. In their method, yarns were represented as inextensible rods, and inter-yarn contacts were explicitly detected and resolved using repulsive forces. Their work was later extended to accelerate contact handling [Kaldor et al. 2010].

Cirio et al. [2014] proposed a different approach for yarn-level cloth simulation based on the EoL discretization of rods of Sueda et al. [2011]. They assumed yarns to be in persistent contact in order to avoid explicit intra-fabric contact handling. Their original method for woven fabrics was later extended to support some types of knits [Cirio et al. 2017]. However, the method remains limited, as yarns are not allowed to cross each other while sliding. Crossing of sliding yarns is fundamental for the simulation of the relaxation process of knit patterns [Leaf et al. 2018]. In our work, we apply our novel EoL method to the simulation of yarn-level cloth, using the model of Cirio et al. as starting point. We leverage the concept of persistent yarn contact to model not only simple intra-fabric contacts as they did, but also more complex intra-fabric contacts present in knit patterns, and inter-fabric contacts resulting from multiple stacked layers of yarn-level cloth. We show that, thanks
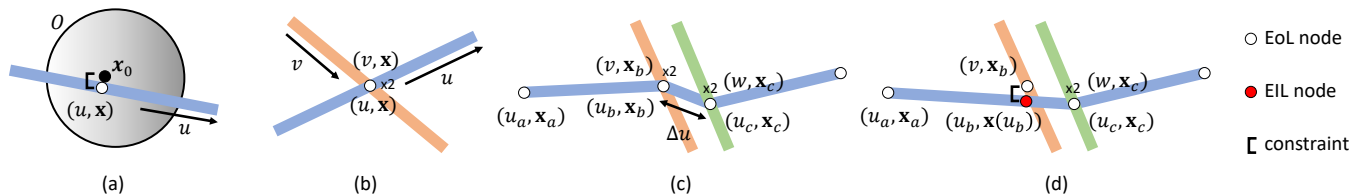
Fig. 2. Examples of mixed Eulerian-Lagrangian discretization of rods. (a) EoL discretization of a rod in sliding contact with an arbitrary object O, proposed by Sueda et al. [2011]. (b) Application of the EoL discretization to sliding rod-rod contact, proposed by Cirio et al. [2014]. (c) Two rods (orange and green) slide on another rod (blue). As the material distance Δu between the contact points gets smaller, forces become infinitely stiff, even in the undeformed case. The degeneracy in the discretization makes the simulation unstable. (d) We propose a novel discretization of sliding rod contacts. When a rod segment is close to degenerate, we replace one EoL node with an EIL node (in red). In this node, the Eulerian coordinate is free, while the Lagrangian coordinates are linearly interpolated. The material distance of the degenerate segment does not participate in the discrete elastic energy of the rod, which results in robust equations.

to our solution, many novel complex phenomena can be accurately and robustly simulated without explicit contact handling.

Yarn-level cloth models are also used in computer graphics to model design and fabrication processes, in particular for knits. Yuksel et al. [2012] created a data structure that enables the construction of knit garments as a tiling procedure. Leaf et al. [2018] introduced a method to predict the visual patterns of complex knits once relaxed, using the yarn-level model of Kaldor et al. [2008]. To alleviate the challenge of explicit contact handling on large cloth patches, they added support for periodic boundary conditions, and simulated small repeated patches. With their method, knit pattern designs can only be studied on flat undeformed configurations. In our work, with our novel EoL-based discretization of yarn-level cloth, we show that we can robustly scale up the size and complexity of knit simulations, and we can analyze complex knit patterns on draped configurations.

Contact Handling of Cloth and Hair Stacks. In cloth and hair simulation, accurate and efficient contact handling has long been one of the major challenges [Bridson et al. 2002]. Our intention is not to cover related work extensively, but to discuss representative works that have paid particular attention to robust handling of cloth or hair stacks.

When multiple cloth layers collide, the exchange of momentum across layers complicates a correct resolution of non-penetration, deformation, and frictional forces together. Non-rigid impact zones [Harmon et al. 2008] simplify the problem by fixing normal motion while enabling tangential sliding. A different approach to enforce robust and accurate contact handling is to turn to asynchronous timestepping [Harmon et al. 2009]. For cloth layers, it is also possible to resolve contact by meshing the inter-layer gaps and preventing mesh inversion [Müller et al. 2015].

In hair assemblies, correct handling of friction plays a key role. One of the challenges is the nonsmooth nature of friction, which requires careful iterative solvers for accurate results [Daviet et al. 2011]. Another challenge is the strong nonlinearity of rod deformation modes to collisions, which requires adaptivity of the iterative solvers for large time stepping [Kaufman et al. 2014]

A different approach to simplify the complexity of hair simulation is to combine features of Eulerian and Lagrangian simulation, in particular Eulerian representations for bulk hair interactions, and Lagrangian representations for detailed contact [McAdams et al.

2009]. Recently, combined Eulerian-Lagrangian methods have also shown success for the robust simulation of stacks of cloth within the Material Point Method. These methods enable accurate Lagrangian tracking of cloth surfaces, plus efficient Eulerian contact handling using a constitutive model of frictional contact [Jiang et al. 2017]. Early methods have been extended to handle rich bending models [Guo et al. 2018].

3 EULERIAN-LAGRANGIAN RODS

In this section, we present a novel mixed Eulerian-Lagrangian discretization of rods. We start with a recap of the regular EoL discretization [Sueda et al. 2011], and its application to yarn-level cloth simulation [Cirio et al. 2014]. Then we discuss the sources of degenerate discretizations and their devastating effects. We conclude with the introduction of our new discretization.

All our exposition refers to the representation of the center line of a rod. The representation of twist is complementary. In our implementation, we use twist-free rods and we assume a homogeneous cross-section, but our approach can be extended to rod representations with twist.

3.1 Eulerian on Lagrangian Discretization

When rods are in contact with other objects, contact points tend to concentrate large local bending, due to the low bending stiffness of the rod and the action of localized external forces. Then, it appears particularly interesting to introduce discretization nodes at contact points, and thus represent efficiently and accurately rod bending. Moreover, if contacts are persistent, using these points in the discretization may simplify overall computations, by avoiding explicit detection and resolution of contacts.

However, contact points may not be stationary in the material domain, due to sliding. To account for the motion of discretization nodes within the material domain, Sueda et al. [2011] introduced the EoL discretization of constrained rods. As shown in Fig. 2-a, a rod node is placed at the contact point between the rod and an arbitrary object O, and its coordinates $(u, \mathbf{x})$ store both Lagrangian (spatial) coordinates $\mathbf{x}$ and Eulerian (material) coordinates u. We use as Eulerian coordinate the undeformed arc length of the rod. With both Eulerian and Lagrangian coordinates, the kinematics of the rod can suffer ambiguities. However, by forcing the rod node to remain at the contact point, its Lagrangian coordinates are constrained, and

the ambiguity is resolved. We denote the contact point on the other object O as $\mathbf{x}_o$, and then, without loss of generality, the constraint on the rod node can be expressed as

$$\mathbf{x} - \mathbf{x}_o = 0. \tag{1}$$

Later, Cirio et al. [2014] considered the particular case of rod-rod contact. Then, the contact point on object O is also an EoL rod node, with Eulerian coordinate v. Moreover, in rod-rod contact, the contact constraint (1) can be enforced implicitly, by making both EoL nodes share their Lagrangian coordinates. In other words, the two EoL nodes have coordinates $(u, \mathbf{x})$ and $(v, \mathbf{x})$, as shown in Fig. 2-b. Another way of looking at the EoL discretization of rod-rod contact is as a 5-dimensional reduced-coordinate formulation.

3.2 Degeneracies and Instabilities

While EoL rod discretizations are beneficial for the efficient and accurate simulation of rods in contact, they are not free of difficulties. Elastic forces become infinitely stiff when two sliding rod nodes get arbitrarily close to each other. Consider the situation shown in Fig. 2-c. The orange and green rods in the figure slide on the blue rod, and approach each other. Their contact points define a blue rod segment with material length $\Delta u = u_c - u_b$ and spatial length $\Delta \mathbf{x} = \|\mathbf{x}_c - \mathbf{x}_b\|$. The stretch energy V_s of a rod segment can be expressed as a function of the ratio between the Lagrangian and Eulerian lengths [Cirio et al. 2014], i.e.,

$$V_s = \frac{1}{2} k_s \, \Delta u \left(\frac{\|\Delta \mathbf{x}\|}{\Delta u} - 1 \right)^2, \tag{2}$$

where k_s is the material stiffness.

In the undeformed case, i.e., $\|\Delta \mathbf{x}\| = \Delta u$, the effective stiffness of the stretch energy with respect to either the Lagrangian or Eulerian length is $\frac{\partial^2 V_s}{\partial \|\Delta \mathbf{x}\|^2} = \frac{\partial^2 V_s}{\partial \Delta u^2} = \frac{k_s}{\Delta u}$. It is evident that as the nodes slide and get closer in the material domain, the stiffness tends to infinity, making simulations unstable.

The problem at hand boils down to a degeneracy in the discretization. The classic approach to avoid degenerate discretizations is to remesh the geometry, as done as well in other EoL methods [Weidner et al. 2018]. In the case of rods, the trivial approach to remeshing is to collapse both adjacent nodes into one. However, this approach is not viable when the nodes represent two sliding contacts. It is paramount to retain the Eulerian coordinates of both nodes in order to determine how the contacts continue sliding. To the best of our knowledge, no prior work on EoL rods shows situations where sliding contacts get arbitrarily close and cross each other. Sueda et al. [2011] showed sliding contact of rods with fixed or rigid bodies; Cirio et al. [2014; 2017] considered rod-rod contact in woven and knitted cloth, but they applied a repulsive force when two contacts were in close proximity; remeshing due to degeneracies was used in EoL cloth [Weidner et al. 2018], but the examples did not exhibit arbitrarily close sliding contacts either. Challenging situations may appear when rods are sandwiched and the contacts cross each other, and this situation cannot be handled by simply collapsing nearby nodes.

3.3 Eulerian with Interpolated Lagrangian Discretization

To robustly handle degenerate discretizations under sliding contact, we introduce another type of mixed Eulerian-Lagrangian node. This node has only a free Eulerian coordinate, as this property is key to correctly capture sliding. Its Lagrangian coordinates, on the other hand, are interpolated between adjacent nodes. We call this node an *Eulerian with Interpolated Lagrangian* node (EIL).

Looking again at Fig. 2-c, we take the node with Eulerian coordinate u_b, and we transform into an EIL node, as shown in Fig. 2-d, with the node highlighted in red. Then, its Lagrangian coordinates are computed through linear interpolation of its adjacent EoL nodes as:

$$\mathbf{x}(u_b) = \frac{u_c - u_b}{u_c - u_a} \, \mathbf{x}_a + \frac{u_b - u_a}{u_c - u_a} \, \mathbf{x}_c. \tag{3}$$

Linear interpolation of the Lagrangian coordinates produces geometric properties that make the EIL node transparent to internal rod forces. There is no bending, hence the node does not participate in any bending energy computation. Stretch is the same on the two adjacent segments, hence stretch energy can be measured between the two adjacent nodes, bypassing the EIL node. As a result, even if the Eulerian distance between the EIL node and its adjacent nodes becomes arbitrarily short, there is no pernicious effect on the numerical stiffness, and the degenerate discretization becomes harmless. Later in Section 4.2, we provide more details about the definition of elastic energy terms.

At an EIL node, the contact constraint (1) can not be enforced trivially, as the Lagrangian coordinates are not free coordinates. Therefore, this constraint must be handled explicitly. In the rod-rod contact shown in Fig. 2-d, this translates into an explicit constraint between $\mathbf{x}(u_b)$, the interpolated position of the EIL node, and $\mathbf{x}_b$, the position of the corresponding EoL node along the orange rod. Through the interpolation (3) of the Lagrangian coordinate on the EIL node, the constraint affects its Eulerian coordinate, and thus it induces sliding despite the degeneracy, as desired. It also affects the motion of the adjacent nodes, and thus it satisfies two-way coupling at the contact. To compute the effect of the constraint on the various free coordinates, we make use of the Jacobian of the linear interpolation (3).

4 ROBUST DISCRETE MECHANICS

In this section, we describe our runtime algorithm to robustly simulate the dynamics of complex arrangements of rods in sliding contact. Our central strategy to avoid instabilities under degenerate discretizations is to replace offending EoL nodes with the novel EIL nodes described in the previous section, and formulate internal rod forces that ignore the EIL nodes. We start the section with a description of the dynamic node assignment, we continue with the formulation of internal and external force terms, and we conclude with the derivation of the equations of motion.

4.1 Node Assignments

On each simulation step, we start by identifying EoL and EIL nodes for all rods in the simulation scene. To do this, we check the material distance between pairs of consecutive nodes along each rod, and we ensure that an EIL node is introduced every time that the distance

is below a safety threshold. We do this efficiently through simple list sorting and traversal operations.

For each step and each rod, let us consider as input a set of nodes defined by their current Eulerian and Lagrangian coordinates $(u, \mathbf{x})$. These nodes may be sliding contacts inherited from the previous step, new contacts detected through collision detection, fixed discretization points along the rod (i.e., with fixed Eulerian coordinate, such as end points), or persistent contacts in the woven or knitted structure of a yarn-level fabric which can be defined at preprocessing.

We initialize all nodes as EoL. Then, we sort the nodes according to their Eulerian coordinates, which yields a sorted sequence $\{(u_i, \mathbf{x}_i)\}, u_i > u_{i-1}$. Next, we traverse the sequence in order. Whenever we find that a node is closer than a safety threshold distance d from the previous node, we tag it as EIL node (In our implementation, the safety distance is $0.1\times$ the length of rest-shape rod segments). In a special case, when the current node has a fixed Eulerian coordinate (e.g., it is an end node), we leave it as EoL node, and we tag as EIL the last EoL node instead. Thanks to this simple node assignment strategy, we ensure that the material distance between any pair of consecutive EoL nodes is above the safety threshold. As EIL nodes are determined based on sorting, they switch when two adjacent nodes actually cross each other. However, this has little effect on the simulation, as the nodes are co-located when they cross. We have not observed noticeable effects due to the EIL selection policy.

We revise the assignment of nodes on every simulation step. More specifically, in our implementation we revise them before the first Newton step of a full nonlinear solve. Switching node assignments to and from EoL and EIL introduces discontinuities in energy and momentum. These discontinuities could be reduced by locally optimizing the Lagrangian and Eulerian coordinates of the nodes in contact. If only the switching node is optimized, we find that simply leaving its Eulerian coordinate unchanged is an optimal solution when strain is uniform and the two incident rod segments are collinear, as shown in the Appendix. We have opted for this simple solution in practice. Furthermore, whenever a node changes its status between two steps from EIL to EoL, we initialize its Lagrangian coordinates according to the contact constraint (1). Energy and momentum discontinuities could also be smoothed by making the transitions progressive within an interval of material distance, but we found that this was not necessary in practice. All our simulations were executed with no smoothing, yet there are no artifacts, despite the ubiquitous node transitions.

4.2 Definition of Force Terms

In our simulations of rods, we consider internal forces that model the resistance of rods to deformation, inter-rod forces that account for yarn-yarn contacts in yarn-level cloth simulation, other external forces due to rod-rod contact between different layers of cloth, or due to additional contacts, plus gravity and damping effects. We focus the attention on internal forces and yarn-yarn contacts. Gravity, damping, and external collisions are unaffected by our proposed discretization. In all cases, we follow the definitions of force terms in previous yarn-level cloth models [Cirio et al. 2014, 2017].

Stretch and bending are defined using discrete strains, which yield strain energy densities that are then integrated along yarn segments. The stretch energy is defined in (2), and the bending energy is rewritten from [Cirio et al. 2014] as

$$V_b = k_b \frac{\theta^2}{\Delta u_1 + \Delta u_2}, \qquad (4)$$

where k_b is the bending stiffness, θ is the angle between two segments, and Δ_1 and Δ_2 are the material lengths of the two segments.

As introduced in Section 3.3, the key to a robust formulation under degeneracies is to avoid EIL nodes in the definition of stretch and bending energy terms. Then, on each simulation step, and for each rod, we traverse the sequence of sorted nodes $\{(u_i, \mathbf{x}_i)\}$, and we define a stretch (resp. bending) energy term for every pair (resp. triple) of consecutive EoL nodes.

The inclusion of EIL nodes also requires the explicit addition of the constraint (1). We enforce this constraint using a soft constraint with large stiffness (In our implementation, $1000\times$ larger than the effective stretch stiffness $\frac{k_s}{\Delta u}$ of rest-shape rod segments). Note that the constraint may be acting between two EIL nodes (one on each rod, if both rods suffer a degeneracy close to their contact), or between an EIL node and an EoL node. For EIL nodes, the force on the interpolated Lagrangian coordinates is mapped to the actual free coordinates through the Jacobian of linear interpolation, as discussed in Section 3.3. We have opted for stiff soft constraints because, in our experience, stiff zero-rest-length springs are comparatively less problematic than other elastic terms. Note that the alternative of hard constraints would yield a complex system of equations, combining Lagrange multipliers with implicit integration of stiff stretch forces. Our constraints are similar to the soft bindings of Sifakis et al. [2007], but we set springs with EIL nodes, which are not fixed in the material domain, while soft bindings set springs between particles and fixed points on a meshed object.

Cirio et al. [2014] proposed to model friction for rod-rod contacts as a trivial anchored spring on Eulerian coordinates. In our case, this force model can be adopted with no changes, as both EoL and EIL nodes retain free Eulerian coordinates. The joint effect of the contact constraint (1) and the friction force is actually the main reason for sliding of contact points, and therefore for the change of the Eulerian coordinates of rod nodes. Thanks to our proposed discretization, with free Eulerian coordinates at EIL nodes, the dynamics of rods are correctly and robustly represented when sliding contacts cross each other. Remeshing through naïve node collapse misses the required free Eulerian coordinates, and does not allow correct sliding.
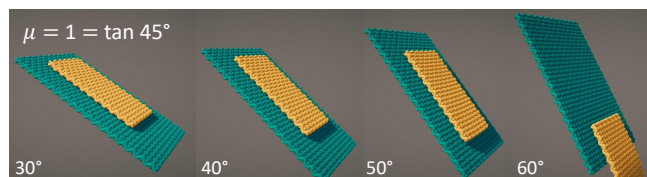
The figure above shows a validation of the friction model and sliding of two patches of cloth. All contacts are handled implicitly using EoL and EIL nodes. The green patch is fixed, and the friction

Nodes:	Lagrangian	EoL Intra-Fabric	EOL Inter-Fabric (max)	EIL (max)	Default step	Sim cost (secs/step)
Tablecloth (Figs. 1 and 7)	1 576	96 290	132 200	79 019	1 ms	15.9
Pocket (Fig. 5)	2 484	398 782	245 024	45 742	1 ms	93.9
Tag (Fig. 6)	1 010	68 810	18 356	4 563	2 ms	18.18
Knit 1 (Fig. 4-left)	184	75 096	–	671	0.5 ms	17.33
Knit 2 (Fig. 4-right)	208	55 520	–	602	0.5 ms	15.53

Table 1. Simulation size and performance for the main examples in the paper. The columns indicate, for each scene: the number of pure Lagrangian nodes (i.e., rod endings), the intra-fabric EoL nodes due to yarn-yarn contacts within a pattern, the maximum inter-fabric EoL nodes to satisfy implicit sliding contact between patches, and the maximum simultaneous EIL nodes to correctly handle discretization degeneracies. The last two columns show the default time step and the average simulation cost per time step.

coefficient with the yellow patch is $\mu = 1$. The yellow patch remains still at inclines below 45 degrees, and slides at steeper inclines, as expected with Coulomb's model.

The simulation of cloth with yarn-level persistent contacts requires special force terms that resist the deformation modes of yarn-yarn contact. These are, for example, shear forces [Cirio et al. 2014] and, in the case of knits, wrapping forces [Cirio et al. 2017]. These forces are defined on Lagrangian coordinates only, with no effect on the material length of yarn segments; therefore, they do not induce robustness problems under degenerate discretizations. For EIL nodes, the force is mapped to the free coordinates in the same way as for the contact constraint discussed above.

The last relevant force is the parallel-yarn contact force, designed by Cirio et al. [2014] to model the inability of some yarns to cross each other within fabric patterns. In our setting, some rod nodes should receive parallel-yarn contact forces as well, but others should not, to allow them to cross each other. We disable parallel-yarn contact forces between a pair of nodes if (a) one of the nodes represents an external contact (e.g., with another fabric), or (b) the two colliding yarns lie on different sides of the rod and they do not bend around the rod. To test if a colliding yarn bends around the rod, we compute a bending vector by averaging the direction vectors of the two incident yarn segments, and we check if the dot product of this bending vector and the contact normal is above a threshold (0.25 in our implementation).

4.3 Mixed Statics-Dynamics

Once that force terms are defined, we can also define inertial terms and derive the equations of motion using the general Euler-Lagrange equations [Goldstein et al. 2002], as done by Sueda et al. [2011] for the original formulation of EoL rods. Lagrangian velocities along a rod are obtained by interpolating Lagrangian velocities of EoL nodes, while EIL nodes are irrelevant in this regard. Since EIL nodes do not affect Lagrangian velocities, they do not affect kinetic energy either. As a corollary, EIL nodes do not carry inertial terms, i.e., they can be considered massless, and then their coordinates are defined through static equilibrium. Therefore, to obtain the kinetic energy of each rod, we traverse the sequence of sorted points $\{(u_i, \mathbf{x}_i)\}$, and we sum a kinetic energy term for each pair of consecutive EoL nodes. For details on the computation of the kinetic energy term of a rod segment and the associated mass submatrix, we refer the reader to [Cirio et al. 2014].

The combined Lagrangian and Eulerian coordinates of the simulation scene form a set of reduced coordinates. We split this set into two: $\mathbf{q}$ are the coordinates of EoL nodes, and $\mathbf{q}_{\text{eil}}$ are the (Eulerian only) coordinates of EIL nodes. We denote as V the total potential energy of the simulation scene, and as $\mathbf{M}$ the mass matrix of EoL nodes. Note that all mass terms of EIL coordinates $\mathbf{q}_{\text{eil}}$ are null. Despite these null terms, the equations of motion can be derived using the general Euler-Lagrange equations. They result in:

$$\mathbf{M}\,\dot{\mathbf{q}} + \nabla_{\mathbf{q}} V = \mathbf{M}\,\dot{\mathbf{q}} + \mathbf{f}\,(\mathbf{q}, \mathbf{q}_{\text{eil}}) = 0; \text{ dynamic} \qquad (5)$$

$$\nabla_{\mathbf{q}_{\text{eil}}} V = \mathbf{f}_{\text{eil}}\,(\mathbf{q}, \mathbf{q}_{\text{eil}}) = 0; \text{ static} \qquad (6)$$

The vector $\mathbf{f}$ (resp. $\mathbf{f}_{\text{eil}}$) represents the forces on EoL nodes (resp. EIL nodes).

As denoted in the equations, there are two distinct sets. EoL nodes are governed by dynamics, while EIL nodes are governed by static equilibrium. Despite this apparent difference, we can safely solve all equations together. We apply implicit Euler integration to the dynamics equations on EoL nodes, and we solve the combined system of equations using Newton's method. We do not resize the system matrix when nodes transition to/from EIL. Instead, we just cancel the matrix rows and columns of the Lagrangian coordinates of EIL nodes.

5 RESULTS

Implementation Details. We have applied our rod simulation method to yarn-level cloth. To this end, we have adapted the GPU solver proposed by Cirio et al. [2014] to handle dynamic rod discretizations. On every simulation step, we first execute the node sorting and assignment operations of Section 4.1, in parallel over all rods. These operations have negligible cost compared to the actual solver. Next, we execute force computations and Jacobian evaluations, parallelized at node level. Note that forces can be referenced to nodes thanks to the linear structure of rods, hence force stencils can be defined implicitly from the node ordering and rod-rod contacts.

For collision detection, we use a sphere packing approach for cloth-cloth collisions and self-collisions, and distance fields for external objects. For non-persistent contacts, we use stiff penalty potentials to resolve collisions.

To determine contacts that require EoL discretization, we combine two strategies. For intra-fabric contacts, we simply use the initial topology of the weave or knit pattern. For inter-fabric contacts, we select the contacts detected by the collision detection step. In our examples, we do this at initialization, as the various layers remain
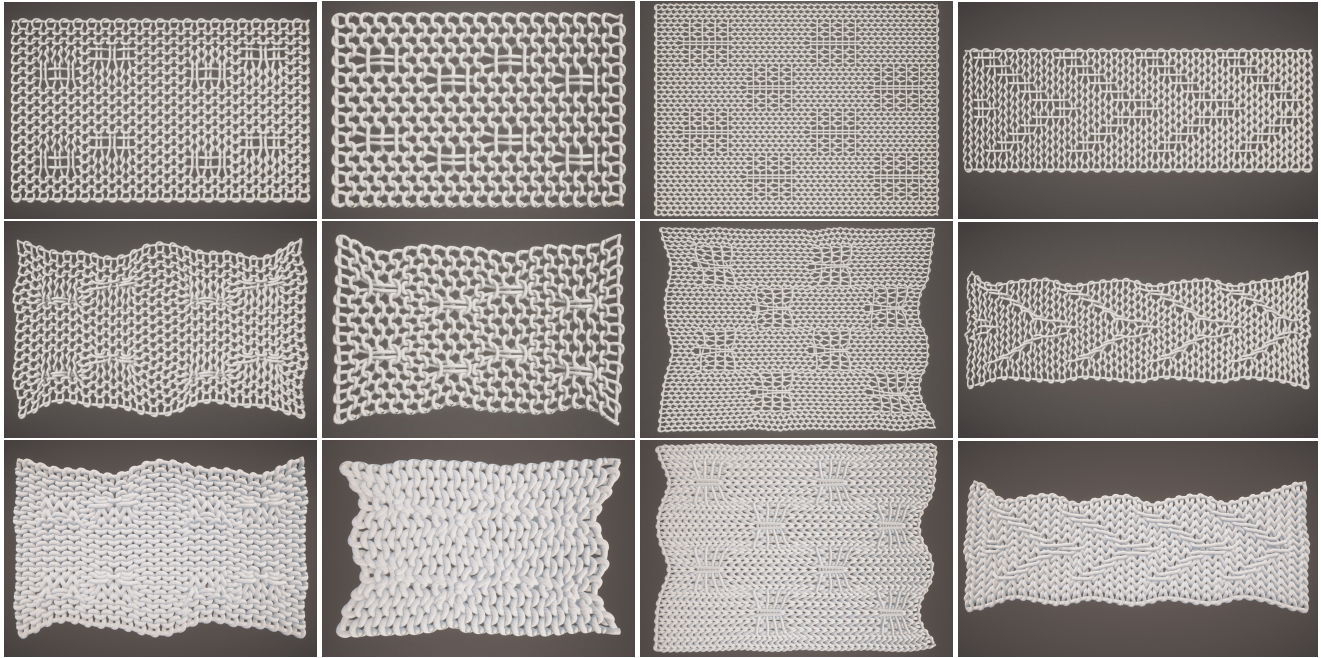
Fig. 3. Four different knit patterns with slip-stitches, where yarn-yarn contacts slide over each other. These examples could not be handled by previous EoL yarn-level methods, and had to resort to purely Lagrangian methods with explicit contact handling. The top row shows the initial configuration for loose knit structures, the middle row the relaxed configuration after simulation of these loose knit structures, and the bottom row the relaxed configuration after simulation of tight knit structures. The three left-most examples are custom structures inspired by those of Leaf et al. [2018], and the rightmost example is a jacquard structure.

in a stacked configuration once initialized. We did not support dynamic addition of EoL contact nodes, as in the examples the cost of collision handling of dynamic contacts was negligible. We did support, however, removal of contact nodes. One obvious reason for removal is that the Eulerian coordinate of a node indicates that it has exit the length of the rod; another reason is that the normal force between two constrained EoL nodes pulls them together instead of pushing, as discussed in [Cirio et al. 2014].
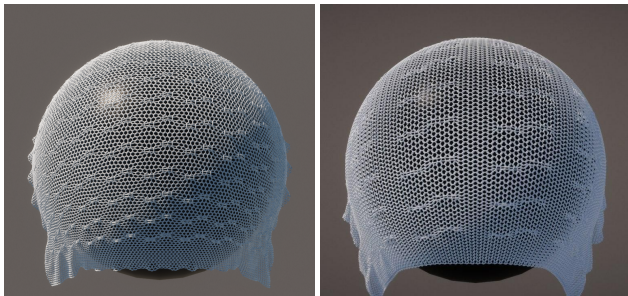

Fig. 4. Two large knit patches draped on a sphere. The knit patterns are drawn from the examples in Fig. 3, and applied to larger patches. Thanks to our EoL formulation, the simulation of these complex knits scales to large sizes without compromising robustness.

Performance. Our simulation examples have been executed on an Intel Core i7-7700K 4-core 4.20 GHz PC with 32 GB of RAM and a Nvidia GeForce GTX 1080 Ti GPU with 11 GB of VRAM.

In Table 1 we show the simulation complexity of the examples shown in the paper. We classify different types of nodes: fully Lagrangian nodes at rod endings, intra-fabric EoL nodes that represent persistent contacts in the topology of the pattern, maximum number of EoL nodes due to inter-fabric contact, and maximum number of simultaneous EIL nodes at any time in the simulation. All simulations run robustly despite the large number of simultaneous EIL nodes, which is an indicator of the number of degenerate rod segments in the scene.

Table 1 also shows the simulation cost for each example, measured in seconds per time step. The default time step ranged from 0.5 ms to 2 ms. We have used adaptive time-stepping to reduce the time step if the Newton solver exhibits bad convergence. The examples occasionally reduce the time step, but they use the default value in the large majority of steps.

Complex Knits. Earlier yarn-level simulation methods assumed a fixed topology of the pattern mesh. This is sufficient for single-layer wovens or simple knits made of knit or purl stitches. However, in multi-layer wovens or complex knits with cables or slip stitches, sliding contacts often sandwich yarns and cross each other. Our rod simulation method enables robust handling of these structures through an efficient EoL approach. In particular, we have tested slip-stitch knit patterns where the slipped yarns can slide when

Fig. 5. Snapshots of a simulation of a jeans back pocket. The scene consists of two layers of yarn-level twill denim fabric, stitched on the sides and at the bottom. We pull from the top and the bottom, inducing sliding of the two layers, as well as wrinkles influenced by the combined material. The full simulation is resolved with implicit contact handling in our EoL formulation, and it has over 645K nodes. When the layers slide, the two groups of sliding warp and weft yarns induce pervasive degeneracies in the discretization. The rightmost image shows the soup of nodes at the top of the pocket, with EIL nodes in red.

Fig. 6. Snapshots of simulations of a shirt neck tag. The tag is roughly 5 times stiffer than the shirt, and is stitched on the sides. We apply different deformations to the underlying shirt fabric, from left to right: horizontal stretch, vertical stretch, shear followed by vertical stretch in the middle, and vertical stretch in the middle followed by horizontal compression of the tag. The difference in stiffness induces sliding of the layers, as well as wrinkling at the interface (see first and third snapshots). The last example shows the separation of the tag as it buckles. We trigger the separation of EoL contacts automatically by checking the sign of the normal force.

the fabric gets deformed. In Fig. 3 we show the relaxation of four different patterns: three custom structures inspired by examples of Leaf et al. [2018], and one jacquard structure. We have tested the four patterns under loose knitting, but also under tight knitting, which produces more complex contact configurations. Both settings are handled robustly.

We program the initial topology of knit patterns using a regular grid of instructions, and we tune the rest-length of slipped yarns to obtain relaxed patterns with different aesthetics. This approach is equivalent to the one followed by Leaf et al. for pattern design. However, with our EoL discretization, we also enable scalable draping of large-scale complex knits. In such case, purely Lagrangian yarn-level models can obviously not exploit patch periodicity, as done by Leaf et al. Fig. 4 shows two large cloth patches draped on a sphere. These patches are stitched using two of the patterns in Fig. 3. The simulations consist of 55K and 75K nodes, with average inter-stitch distances of just 0.8 mm.

Multiple Layers of Yarn-Level Cloth. Cloth often appears stacked in layers, either different garments on top of each other, or panels of the same garment stitched together. When contact between the layers persists over time, even if the layers slide relative to each other, the EoL approach offers an attractive way to simulate cloth deformation without explicit contact handling. We have evaluated the performance of our method when applied to the simulation of multiple layers of yarn-level cloth. The rods of the various layers pile

up in complex contact arrangements, and require constant updates to the discretization to correctly handle the pervasive degeneracies.

Fig. 5 shows snapshots of a simulation of a jeans back pocket. The scene consists of two layers of twill denim fabric, stitched on the sides and at the bottom. The fabric is modeled at the yarn-level at a realistic resolution, with 44 yarns per inch. This yields a total of 645K nodes. We pull the pocket from the top and the bottom, inducing sliding of the two layers. When the tension grows, the lateral compression produces fine wrinkles that conform to the two layers of fabric.

Fig. 6 shows snapshots of a simulations of a shirt neck tag. The tag is stitched to the underlying shirt fabric on the sides. It is roughly 5 times stiffer than the shirt; therefore, when we pull from the fabric of the shirt, the deformation suffers a discontinuity at the boundary of the tag. The snapshots show horizontal stretch, vertical stretch, shear followed by vertical stretch in the middle, and vertical stretch in the middle followed by horizontal compression of the tag. Notice in the second and third snapshots visible sliding of the two layers, and in the first and third snapshots wrinkles next to the boundary of the tag due to the differences in material combined with sliding. The last snapshot also shows the tag separating as it buckles. In this last snapshot, the simulation begins by stretching the underlying cloth, and the EoL representation resolves the sliding motion of the two layers without the need for explicit contact handling. Then, we compress the tag, which buckles and produces sticking forces at EoL contacts. We trigger automatically the removal of EoL contact constraints, allowing the tag to separate.
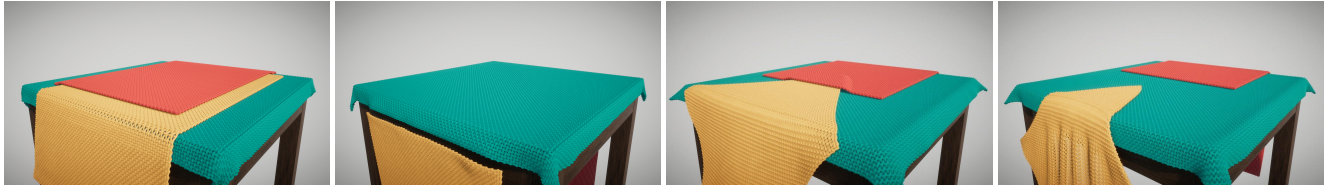
Fig. 7. Similar scenes to the one in Fig. 1, but with no friction between the tablecloths, and in two different arrangements. Two left-most images: aligned tablecloths. Two right-most images: tablecloths at an angle. Despite continuous sliding and changes to the discretization, the green tablecloth remains perfectly on the table. Sliding is smooth and robust both when the tablecloths are aligned or at an angle. In the left scene, the number of simultaneous EIL nodes can be as high as 34% of the total nodes.

Fig. 1 and Fig. 7 show two simulations of stacked tablecloth layers with different friction properties. The tablecloths are modeled as thick-yarn plain weaves, with an inter-yarn separation of 5.6 mm, and yarn radius of 2.25 mm. In this scene, we also added EoL nodes at the edge of the table, to enable smooth sliding on sharp features. As described by Weidner et al. [2018], the tablecloths suffer energy discontinuities or even get stuck if we do not do so. With three stacked layers, the number of simultaneous EIL nodes can be as high as 34% of the total nodes. The figures also show close-ups of the discretizations at particular instants in time. As evidenced in the accompanying video, the discretizations change constantly. Despite continuous sliding and changes to the discretization, our simulation method handles contact and friction correctly. Note that friction is controlled simply through the Coulomb coefficient of the Eulerian anchor force (see Section 4.2 and [Cirio et al. 2014]). In the frictionless case shown in Fig. 7, the green tablecloth remains perfectly on the table.

6 DISCUSSION AND FUTURE WORK

In this paper, we have extended EoL rod simulation to handle robustly complex contact arrangements with multiple stacked rods, and sliding and crossing contacts. As shown in our experiments, these conditions appear in diverse practical scenarios, including the simulation of complex knits, and contact between multiple layers of cloth. Our solution handles ubiquitous discretization degeneracies in a simple and elegant manner, and its implementation brings only small changes to previous methods.

In the development of our method and implementation, we have identified several limitations as well as opportunities for further investigation. As discussed in Section 4.1, switching node assignments to and from EoL and EIL introduces discontinuities in energy and momentum. These discontinuities did not turn into artifacts in our examples, but perhaps they affected mildly the convergence of the Newton solve. Smoothing these discontinuities is possible, by locally optimizing the Lagrangian and Eulerian coordinates of switching nodes, or by making node transitions progressive.

In the examples, we did not implement dynamic addition of EoL nodes. It is not evident when this could turn beneficial or not. It would be necessary to design some metric that compares simulation accuracy and/or robustness with or without the addition of EoL nodes at contacts, and then use this metric to guide the addition of new EoL nodes.

The contact constraint of EoL and/or EIL nodes ignores the thickness of rods. However, this thickness should be accounted for in the computation of bending forces. We currently add the thickness as postprocessing for rendering, and the same procedure could be followed at runtime for force computation.

Our knit relaxation examples demonstrate the ability of EoL methods to support complex and tight knits with yarn sliding. However, some cases may be difficult to handle due dynamic creation of contacts. In such cases, one could use a purely Lagrangian method [Leaf et al. 2018] for the initial relaxation of the yarn structure, followed by our EoL method for dynamic simulation of larger patches or garments.

We have demonstrated our solution on patches of cloth simulated fully at yarn level. Such full yarn-level detail appears particularly relevant in our complex knit examples, to correctly capture sliding of slip-stitches. However, in other examples the simulation cost could be reduced drastically by considering yarn-level detail only when and where necessary.

To conclude, we think it is worth to explore the main ideas of our work beyond rods, for EoL formulations on other domains, such as thin-shell cloth [Weidner et al. 2018]. A key insight of our method is to avoid remeshing, and turn EoL nodes into EIL nodes when the discretization becomes degenerate. The extension of EIL nodes to other domains may be simple, but our node assignment algorithm is tied to the linear domain of rods.

ACKNOWLEDGMENTS

REFERENCES

Miklós Bergou, Basile Audoly, Etienne Vouga, Max Wardetzky, and Eitan Grinspun. 2010. Discrete Viscous Threads. *ACM Trans. Graph.* 29, 4, Article Article 116 (2010), 10 pages.

Miklós Bergou, Max Wardetzky, Stephen Robinson, Basile Audoly, and Eitan Grinspun. 2008. Discrete Elastic Rods. *ACM Trans. Graph.* 27, 3 (2008), 1–12.

Florence Bertails, Basile Audoly, Marie-Paule Cani, Bernard Querleux, Frédéric Leroy, and Jean-Luc Lévundefinedque. 2006. Super-Helices for Predicting the Dynamics of

Natural Hair. *ACM Trans. Graph.* 25, 3 (2006), 1180–1187.

Robert Bridson, Ronald Fedkiw, and John Anderson. 2002. Robust Treatment of Collisions, Contact and Friction for Cloth Animation. *ACM Trans. Graph.* 21, 3 (2002), 594–603.

Gabriel Cirio, Jorge Lopez-Moreno, David Miraut, and Miguel A. Otaduy. 2014. Yarn-level Simulation of Woven Cloth. *ACM Trans. Graph.* 33, 6 (Nov. 2014), 207:1–207:11.

Gabriel Cirio, Jorge Lopez-Moreno, and Miguel A Otaduy. 2017. Yarn-level cloth simulation with sliding persistent contacts. *IEEE transactions on visualization and computer graphics* 23, 2 (2017), 1152–1162.

Gilles Daviet, Florence Bertails-Descoubes, and Laurence Boissieux. 2011. A Hybrid Iterative Solver for Robustly Capturing Coulomb Friction in Hair Dynamics. In *Proceedings of the 2011 SIGGRAPH Asia Conference (SA '11)*. Association for Computing Machinery, New York, NY, USA, Article Article 139, 12 pages.

Ye Fan, Joshua Litven, David I. W. Levin, and Dinesh K. Pai. 2013. Eulerian-on-Lagrangian Simulation. *ACM Trans. Graph.* 32, 3, Article Article 22 (2013), 9 pages.

Herbert Goldstein, Charles Poole, and John Safko. 2002. Classical mechanics.

Qi Guo, Xuchen Han, Chuyuan Fu, Theodore Gast, Rasmus Tamstorf, and Joseph Teran. 2018. A Material Point Method for Thin Shells with Frictional Contact. *ACM Trans. Graph.* 37, 4, Article Article 147 (2018), 15 pages.

David Harmon, Etienne Vouga, Breannan Smith, Rasmus Tamstorf, and Eitan Grinspun. 2009. Asynchronous Contact Mechanics. In *ACM SIGGRAPH 2009 Papers (SIGGRAPH '09)*. Association for Computing Machinery, New York, NY, USA, Article 87, 12 pages.

David Harmon, Etienne Vouga, Rasmus Tamstorf, and Eitan Grinspun. 2008. Robust Treatment of Simultaneous Collisions. *ACM Trans. Graph.* 27, 3 (2008), 1–4.

Hayley Iben, Mark Meyer, Lena Petrovic, Olivier Soares, John Anderson, and Andrew Witkin. 2013. Artistic simulation of curly hair. In *Proceedings of the 12th ACM SIGGRAPH/Eurographics Symposium on Computer Animation*. Association for Computing Machinery, New York, NY, USA, 63–71.

Chenfanfu Jiang, Theodore Gast, and Joseph Teran. 2017. Anisotropic Elastoplasticity for Cloth, Knit and Hair Frictional Contact. *ACM Trans. Graph.* 36, 4, Article Article 152 (2017), 14 pages.

Jonathan M Kaldor, Doug L James, and Steve Marschner. 2008. Simulating knitted cloth at the yarn level. *ACM Transactions on Graphics (TOG)* 27, 3, Article 65 (2008), 9 pages.

Jonathan M Kaldor, Doug L James, and Steve Marschner. 2010. Efficient yarn-based cloth with adaptive contact linearization. *ACM Transactions on Graphics (TOG)* 29, 4, Article 105 (2010), 10 pages.

Danny M. Kaufman, Rasmus Tamstorf, Breannan Smith, Jean-Marie Aubry, and Eitan Grinspun. 2014. Adaptive Nonlinearity for Collisions in Complex Rod Assemblies. *ACM Trans. Graph.* 33, 4, Article Article 123 (July 2014), 12 pages. https://doi.org/10.1145/2601097.2601100

Jonathan Leaf, Rundong Wu, Eston Schweickart, Doug L. James, and Steve Marschner. 2018. Interactive Design of Periodic Yarn-Level Cloth Patterns. *ACM Trans. Graph.* 37, 6, Article 202 (2018), 15 pages.

Duo Li, Shinjiro Sueda, Debanga R. Neog, and Dinesh K. Pai. 2013. Thin Skin Elastodynamics. *ACM Trans. Graph.* 32, 4, Article 49 (2013), 10 pages.

Aleka McAdams, Andrew Selle, Kelly Ward, Eftychios Sifakis, and Joseph Teran. 2009. Detail Preserving Continuum Simulation of Straight Hair. *ACM Trans. Graph.* 28, 3, Article Article 62 (2009), 6 pages.

Matthias Müller, Nuttapong Chentanez, Tae-Yong Kim, and Miles Macklin. 2015. Air Meshes for Robust Collision Handling. *ACM Trans. Graph.* 34, 4, Article 133 (2015), 9 pages.

Dinesh K. Pai. 2002. STRANDS: Interactive Simulation of Thin Solids using Cosserat Models. *Computer Graphics Forum* 21, 3 (2002), 347–352.

Robert E. Rosenblum, Wayne E. Carlson, and Edwin R. Tripp. 1991. Simulating the structure and dynamics of human hair: Modelling, rendering and animation. *Journal of Visualization and Computer Animation* 2 (1991), 141–148.

Prashant Sachdeva, Shinjiro Sueda, Susanne Bradley, Mikhail Fain, and Dinesh K Pai. 2015. Biomechanical simulation and control of hands and tendinous systems. *ACM Transactions on Graphics (TOG)* 34, 4, Article 42 (2015), 10 pages.

Andrew Selle, Michael Lentine, and Ronald Fedkiw. 2008. A mass spring model for hair simulation. *ACM Transactions on Graphics (TOG)* 27, 3, Article 64 (2008), 11 pages.

Martin Servin, Claude Lacoursiere, Fredrik Nordfelth, and Kenneth Bodin. 2010. Hybrid, multiresolution wires with massless frictional contacts. *IEEE transactions on visualization and computer graphics* 17, 7 (2010), 970–982.

Eftychios Sifakis, Tamar Shinar, Geoffrey Irving, and Ronald Fedkiw. 2007. Hybrid Simulation of Deformable Solids. In *Proceedings of the 2007 ACM SIGGRAPH/Eurographics Symposium on Computer Animation (SCA '07)*. Eurographics Association, 81–90.

J. Spillmann and M. Teschner. 2007. CoRdE: Cosserat Rod Elements for the Dynamic Simulation of One-Dimensional Elastic Objects. In *Proceedings of the 2007 ACM SIGGRAPH/Eurographics Symposium on Computer Animation (SCA '07)*. Eurographics Association, Goslar, DEU, 63–72.

Jonas Spillmann and Matthias Teschner. 2008. An adaptive contact model for the robust simulation of knots. *Computer Graphics Forum* 27, 2 (2008), 497–506.

Shinjiro Sueda, Garrett L. Jones, David I. W. Levin, and Dinesh K. Pai. 2011. Large-scale Dynamic Simulation of Highly Constrained Strands. *ACM Trans. Graph.* 30, 4 (2011), 39:1–39:10.

Nicholas J Weidner, Kyle Piddington, David IW Levin, and Shinjiro Sueda. 2018. Eulerian-on-lagrangian cloth simulation. *ACM Transactions on Graphics (TOG)* 37, 4, Article 50 (2018), 11 pages.

Cem Yuksel, Jonathan M Kaldor, Doug L James, and Steve Marschner. 2012. Stitch meshes for modeling knitted clothing with yarn-level detail. *ACM Transactions on Graphics (TOG)* 31, 4, Article 37 (2012), 12 pages.

A NODE TRANSITION BETWEEN EOL AND EIL

Consider a node with Eulerian coordinate u_b, which transitions from EoL (as in Fig. 2-c) to EIL (as in Fig. 2-d) and vice versa. This transition produces a discontinuity in the local energy. Under certain assumptions, the discontinuity can be minimized through a closed-form optimization of the Eulerian coordinate u_b. In this optimization, we assume that the matching node $(v, \mathbf{x}_b)$ remains fixed, and we consider only stretch energies.

In the transition from EIL to EoL, the Lagrangian coordinate moves from $\mathbf{x}(u_b)$ to $\mathbf{x}_b$, to join the matching node. This jump introduces stretch energy, which can be minimized by making stretch uniform across the new EoL node. Then, the optimal Eulerian coordinate can be computed as

$$u_b \leftarrow \frac{\|\mathbf{x}_b - \mathbf{x}_c\| \, u_a + \|\mathbf{x}_a - \mathbf{x}_b\| \, u_c}{\|\mathbf{x}_a - \mathbf{x}_b\| + \|\mathbf{x}_b - \mathbf{x}_c\|}. \tag{7}$$

In the transition from EoL to EIL, the Lagrangian coordinate is now interpolated from $\mathbf{x}_a$ and $\mathbf{x}_c$. This jump introduces a non-zero energy in the newly created soft-constraint with $\mathbf{x}_b$. This energy can be minimized by placing $\mathbf{x}(u_b)$ on the closest point to $\mathbf{x}_b$ along the segment between $\mathbf{x}_a$ and $\mathbf{x}_c$. Then, the optimal Eulerian coordinate can be computed as

$$u_b \leftarrow \max\left(\frac{(\mathbf{x}_a - \mathbf{x}_c)^T (\mathbf{x}_b - \mathbf{x}_c) \, u_a + (\mathbf{x}_a - \mathbf{x}_c)^T (\mathbf{x}_a - \mathbf{x}_b) \, u_c}{(\mathbf{x}_a - \mathbf{x}_c)^T (\mathbf{x}_a - \mathbf{x}_c)}, u_c \right). \tag{8}$$

This result can also be expressed as a function of the angle θ between the rod segments $(\mathbf{x}_a - \mathbf{x}_b)$ and $(\mathbf{x}_b - \mathbf{x}_c)$:

$$u_b \leftarrow \max\left(\frac{w_a \, u_a + w_c \, u_c}{w_a + w_c}, u_c \right), \tag{9}$$

with $w_a = \|\mathbf{x}_b - \mathbf{x}_c\|^2 + \|\mathbf{x}_a - \mathbf{x}_b\| \, \|\mathbf{x}_b - \mathbf{x}_c\| \, \cos\theta$,

and $w_c = \|\mathbf{x}_a - \mathbf{x}_b\|^2 + \|\mathbf{x}_a - \mathbf{x}_b\| \, \|\mathbf{x}_b - \mathbf{x}_c\| \, \cos\theta$.

Furthermore, with uniform stretch in both segments, the result can be expressed as a function of the Eulerian coordinates alone:

$$w_a = (u_b - u_c)^2 + (u_a - u_b)(u_b - u_c) \cos\theta, \tag{10}$$

$$w_c = (u_a - u_b)^2 + (u_a - u_b)(u_b - u_c) \cos\theta.$$

Then, it is easy to see that, as the segments become collinear, i.e., $\theta \to 0$, the optimal result is to simply leave the Eulerian coordinate u_b of the EIL node unchanged.